JOURNAL OF PROPULSION AND POWER
Vol. 15, No. 5, September–October 1999

Vane Row Indexing for Passive Vibration Control of Axial-Flow Turbomachine Rotors

Albert J. Sanders* and Sanford Fleeter†
Purdue University, West Lafayette, Indiana 47907

A mathematical model is developed to analyze vane row indexing for passive flow-induced vibration control. A compressible flat-plate cascade analysis is extended to account for the induced velocities due to the potential fields of adjacent blade rows. Then, this model is applied to a baseline stator–rotor–stator configuration with the effects of Mach number, steady vane loading, and axial spacing investigated. For the particular geometry analyzed, the minimum unsteady lift and maximum unsteady moment responses occur near the unindexed position of the stator vane rows; simply decreasing the axial spacing markedly affects the rotor-blade unsteady aerodynamic response. However, by indexing the stator vanes, significant reductions in the unsteady lift and moment are achieved at the close spacings. At the closest spacing, near complete cancellation of the unsteady lift is possible at low Mach numbers. At high Mach numbers, there are optimum combinations of upstream and downstream rotor–stator axial spacings, which can result in complete cancellation of the unsteady lift, with significant reductions in the unsteady lift possible even for a moderate axial spacing of 30% chord.

Nomenclature

C = airfoil chord length
C_L = unsteady lift coefficient
C_M = unsteady moment coefficient
k = reduced frequency based on chord
k_η = tangential wave number
k_ξ = axial wave number
M = Mach number
$\bar{p}$ = complex amplitude of perturbation pressure
S = tangential spacing of airfoil row
U_w = rotor wheel speed
U_∞ = axial component of freestream velocity
$\bar{u}$ = complex amplitude of axial velocity perturbation
V_∞ = tangential component of freestream velocity
$\bar{v}$ = complex amplitude of tangential velocity perturbation
W_∞ = freestream velocity
$\bar{w}$ = complex amplitude of upwash velocity
$\Delta\bar{p}$ = unsteady pressure difference, upper minus lower
$\Delta\eta$ = phase-shifting constant
$\Delta\xi$ = axial spacing between airfoil rows
η = tangential coordinate
ξ = axial coordinate
σ = interblade phase angle
$\bar{\Phi}$ = complex amplitude of perturbation velocity potential

Subscripts

dn = perturbation due to downstream vane-row potential field
r = quantity associated with rotor blades
s = quantity associated with stator vanes
up = perturbation due to upstream vane-row potential field
w = perturbation due to upstream vane-row viscous wake

Introduction

MULTISTAGE axial-flow turbomachines often are plagued by flow-induced vibrations resulting from unsteady aerodynamic interactions between adjacent blade rows. These vibrations occur when a periodic forcing function, with a frequency at or near one of the airfoil natural frequencies, acts on a particular blade row. For multistage axial-flow turbomachines, each embedded blade row is subjected to three distinct forcing functions: the viscous wakes shed by an upstream airfoil row and the potential flowfields of both upstream and downstream airfoil rows (Fig. 1).

Viscous wakes are velocity deficits resulting from the boundary layers on an upstream airfoil row. These vortical disturbances convect with the mean flow and decay very slowly with distance, usually persisting for several airfoil chord lengths downstream. The potential field is a steady circumferentially nonuniform disturbance that results from the thickness and lifting properties of the blading. This type of disturbance decays exponentially with axial distance, extending both upstream and downstream of each airfoil row. Because of the rapid decay rate, potential field interactions only become significant for closely spaced blade rows, whereas wake interactions occur even when the blade rows are spaced several airfoil chord lengths apart.

To reduce engine size and weight, the current trend in compressor and turbine design is toward decreased axial spacings between adjacent blade rows, with fewer stages and increased airfoil loadings. Unfortunately, these trends have led to increased occurrences of flow-induced vibrations of the blading as a result of the strong unsteady aerodynamic interactions that occur between such closely spaced blade rows.

Dring et al.[1] experimentally investigated the interaction between an axial-flow turbine nozzle and rotor for axial spacings of 15 and 65% of the nominal axial chord. At the close spacing, the potential field of the downstream rotor had a considerable influence on the upstream nozzle row, with the pressure fluctuations being as high as 15% of the dynamic pressure at the stage exit. In addition, the fluctuating pressure at the leading edge of the downstream rotor was found to be as high as 80% of the inlet dynamic pressure. When the axial spacing was increased, the fluctuating pressure on the rotor decreased, typically by a factor of 2. The performance of the turbomachine also is influenced by the spacing between the adjacent blade rows, with a decreased axial spacing resulting in increased efficiency and pressure rise of a low-speed research compressor.[2]

When equal stator vane counts are utilized in successive stages, the stationary vane rows can be indexed relative to one another to minimize the adverse effects of these unsteady interactions. Walker and Oliver[3] indexed the inlet guide vane row of a $1\frac{1}{2}$-stage axial-flow compressor relative to the downstream stator and achieved a 6-dB

Received 31 May 1997; revision received 17 March 1999; accepted for publication 18 March 1999.

*Research Assistant, School of Mechanical Engineering, 1003 Chaffee Hall. Student Member AIAA.
†McAllister Distinguished Professor, School of Mechanical Engineering, 1003 Chaffee Hall. Associate Fellow AIAA.

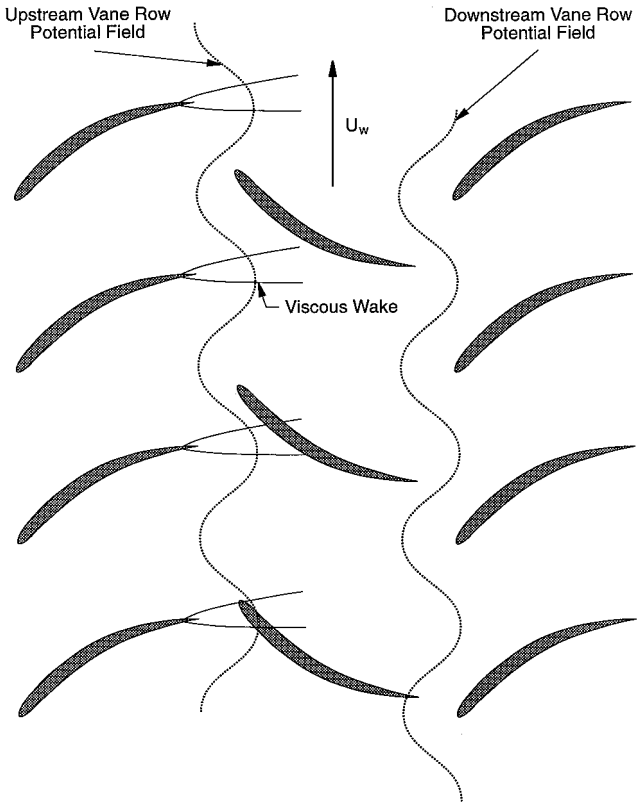

Fig. 1 Unsteady aerodynamic forcing functions to a multistage rotor.

reduction in the inlet noise. The noise reduction was attributed to a combination of sound-wave interference and reduced airfoil surface fluctuating pressures due to wake cancellation. Schmidt and Okiishi[4] achieved an 11.5-dB reduction in the overall sound pressure level in the inlet of a three-stage low-speed research compressor through circumferential vane-row indexing. Additionally, the average stationary flow pattern around the compressor annulus was found to be dependent on the circumferential positions of the stationary vane rows relative to one another. Capece and Fleeter[5] found that indexing the stators of a three-stage research compressor significantly altered the unsteady aerodynamic forcing-function waveforms to the downstream stator vanes. The indexing primarily affected the chordwise gust; indexing of the first-stage stator even affected the response of the third-stage vane row. Dorney and Sharma[6] investigated vane-row indexing effects on performance in a $1\frac{1}{2}$-stage axial-flow turbine using an unsteady two-dimensional viscous flow analysis. They found that indexing the second-stage vane row resulted in changes of up to 2% in efficiency; the second-stage stator experienced significantly more unsteadiness at the maximum efficiency indexing position.

In summary, closely spaced blade rows can result in improved performance and efficiency while reducing both engine size and weight. However, these closely spaced blade rows can lead to unacceptable vibratory stress levels. This paper presents a mathematical model to analyze vane-row indexing for passive control of rotor-blade flow-induced vibrations in multistage axial-flow turbomachines. This is accomplished by extending the compressible flat-plate cascade analysis by Smith[7] to account for the induced velocities due to the potential fields of adjacent airfoil rows. Because the analysis is linear, the rotor-blade response is the superposition of the responses to each individual forcing function, i.e., the potential flowfields of the upstream and downstream vane rows and the viscous wakes shed by the upstream vanes. By indexing the stator vane rows relative to one another, the phase angle of the harmonic rotor-blade response to the potential field of the downstream vane row is altered. Thus, by properly indexing the vane rows, the total response of the rotor blades to all three forcing functions can be minimized.

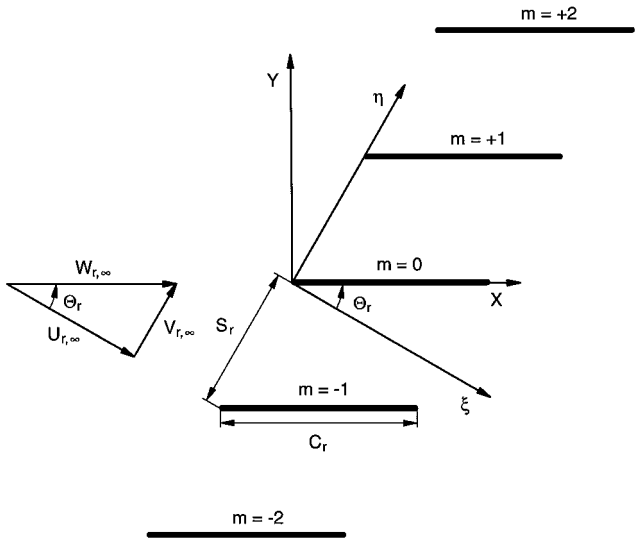

Fig. 2 Flat-plate cascade geometry.

Rotor-Blade Unsteady Analysis

The linear theory model to predict the unsteady aerodynamic loading on the rotor blades due to their interaction with the adjacent vane rows considers a two-dimensional flat-plate airfoil cascade in a subsonic inviscid isentropic irrotational flowfield (Fig. 2). The unsteady flow is assumed to be a small perturbation to the uniform mean flow, leading to the following linearized continuity and momentum equations:

$$\frac{\partial p}{\partial t} + U_{r,\infty}\frac{\partial p}{\partial \xi} + V_{r,\infty}\frac{\partial p}{\partial \eta} + \rho_\infty a_\infty^2\left(\frac{\partial u}{\partial \xi} + \frac{\partial v}{\partial \eta}\right) = 0 \tag{1}$$

$$\frac{\partial u}{\partial t} + U_{r,\infty}\frac{\partial u}{\partial \xi} + V_{r,\infty}\frac{\partial u}{\partial \eta} + \frac{1}{\rho_\infty}\frac{\partial p}{\partial \xi} = 0 \tag{2a}$$

$$\frac{\partial v}{\partial t} + U_{r,\infty}\frac{\partial v}{\partial \xi} + V_{r,\infty}\frac{\partial v}{\partial \eta} + \frac{1}{\rho_\infty}\frac{\partial p}{\partial \eta} = 0 \tag{2b}$$

where the isentropic speed of sound has been used in the continuity equation, $U_{r,\infty}$ and $V_{r,\infty}$ are the steady rotor relative freestream velocity components in the axial ξ and tangential η directions, u and v are the corresponding unsteady perturbation velocity components, and p is the perturbation pressure.

The unsteady flow is harmonic in space and time:

$$p = \bar{p}\exp[i(k_\xi \xi + k_\eta \eta + \omega t)] \tag{3a}$$

$$u = \bar{u}\exp[i(k_\xi \xi + k_\eta \eta + \omega t)] \tag{3b}$$

$$v = \bar{v}\exp[i(k_\xi \xi + k_\eta \eta + \omega t)] \tag{3c}$$

where the complex constants $\bar{p}$, $\bar{u}$, and $\bar{v}$, the axial and tangential wave numbers k_ξ and k_η, and the frequency ω are to be determined.

Substituting these harmonic solutions into the linearized continuity and momentum equations results in the following characteristic equation, which has two solution families:

$$(\omega + U_{r,\infty}k_\xi + V_{r,\infty}k_\eta)\left[(\omega + U_{r,\infty}k_\xi + V_{r,\infty}k_\eta)^2 - a_\infty^2\left(k_\xi^2 + k_\eta^2\right)\right] = 0 \tag{4}$$

With $(\omega + U_{r,\infty}k_\xi + V_{r,\infty}k_\eta) = 0$, the solution corresponds to a vorticity wave that is simply convected with the mean flow with no associated static pressure fluctuation. The axial wave number for this type of disturbance is

$$k_\xi = -\frac{(\omega/a_\infty + k_\eta M_r \sin\Theta_r)}{M_r \cos\Theta_r} \tag{5}$$

If $(\omega + U_{r,\infty}k_\xi + V_{r,\infty}k_\eta)^2 - a_\infty^2(k_\xi^2 + k_\eta^2) = 0$, the solution corresponds to a pair of irrotational pressure waves, one propagating upstream and the other downstream at the speed of sound. The axial wave numbers for these pressure waves are

$$k_\xi = \frac{M_r \cos\Theta_r(\omega/a_\infty + k_\eta M_r \sin\Theta_r) \pm \sqrt{(\omega/a_\infty + k_\eta M_r \sin\Theta_r)^2 - \left(1 - M_r^2\cos^2\Theta_r\right)k_\eta^2}}{1 - M_r^2\cos^2\Theta_r} \tag{6}$$

When the argument under the radical is positive, the axial wave number is real and the waves propagate away from the cascade unattenuated. If the argument is negative, the waves decay exponentially. With the argument zero, only one wave is created, propagating in the tangential direction. This is an acoustic resonance condition also known as cutoff.

The tangential wave number is determined from unsteady periodicity requirements:

$$k_\eta = \frac{\sigma - 2\pi r}{S_r}, \qquad r = 0, \pm1, \pm2, \ldots \tag{7}$$

where the interblade phase angle σ specifies the time lag between unsteady phenomena on adjacent airfoils. Note that σ is a function of the number of unsteady disturbances and the number of airfoils in the responding blade row, specifically,

$$\sigma = +2\pi(N_s/N_r) = +2\pi(S_r/S_s)$$

where N_r is the number of rotor blades with tangential spacing S_r and N_s is the number of stator vanes in the upstream and downstream vane rows with tangential spacing S_s.

The unsteadiness due to blade-row interactions is attributed to both the vortical wakes and the potential flowfields generated by the airfoils in the adjacent vane rows. With S_s the tangential spacing of the vane rows that generate the forcing functions, the forcing function frequency is $\omega = 2\pi(U_w/S_s)$, where U_w is the rotor wheel speed. The stage geometry thus fixes the reduced frequency

$$k = \frac{\omega C_r}{W_{r,\infty}} = 2\pi\frac{S_r}{S_s}\frac{C_r}{S_r}\frac{\sin(\Theta_s - \Theta_r)}{\cos\Theta_s}$$

The unsteady aerodynamic loading is modeled by replacing each airfoil in the cascade representation of the rotor with an unsteady bound vorticity distribution. This cascade vorticity wave solution is built up from the fundamental unsteady pressure and vorticity wave solutions, resulting in the following singular integral equation:

$$-\bar{w}(x_0) = \frac{1}{C_r}\int_0^{C_r} \gamma(x) K\left(\frac{x_0 - x}{C_r}\right)\mathrm{d}x \tag{8}$$

where $\bar{w}(x_0)$ is the complex amplitude of the unsteady upwash velocity generated by the adjacent vane rows, $\gamma(x)$ is the unknown bound vorticity, and $K[(x_0 - x)/C_r]$ is a kernel function.[7]

Once the upwash velocity is specified, the corresponding unsteady bound vorticity distribution is determined by collocation and matrix inversion subject to the Kutta condition at the trailing edge. The unsteady pressure at any point in the flowfield is obtained by integrating the linearized momentum equation (2). The following equation for the unsteady pressure difference across the reference airfoil is obtained by applying this equation at a point on the streamlines just above and below the airfoil surface, subtracting the resulting expressions, and simplifying[7]:

$$\Delta\bar{p} = \rho_\infty W_{r,\infty}\gamma \tag{9}$$

where $\Delta\bar{p} = \bar{p}_+ - \bar{p}_-$, with plus or minus referring to the upper or lower airfoil surfaces, respectively. Then, the unsteady lift and moment acting on the blading are calculated from this by integration.

Interaction Upwash Velocity Fields

The boundary value problem is complete once the upwash velocities corresponding to the potential fields of the upstream and downstream vane rows and the viscous wakes shed by the upstream vanes are specified. The upwash induced by the potential field is derived by considering a steady two-dimensional compressible irrotational flowfield, described by the steady perturbation velocity potential equation

$$\left(1 - M_{s,\xi}^2\right)\frac{\partial^2\Phi}{\partial\xi^2} + \left(1 - M_{s,\eta}^2\right)\frac{\partial^2\Phi}{\partial\eta^2} - 2M_{s,\xi}M_{s,\eta}\frac{\partial^2\Phi}{\partial\xi\,\partial\eta} = 0 \tag{10}$$

where M_s is the Mach number of the flow through the stator vane row.

For subsonic flow, this equation has solutions that are periodic in the tangential direction and decay exponentially in the axial direction:

$$\Phi = \sum_{n=1}^{\infty}\bar{\Phi}_n \exp[i(k_\xi\xi + k_\eta\eta)] \tag{11}$$

where the real part of the complex expression is implied, n is the harmonic index, $\bar{\Phi}_n$ is a complex constant, $k_\eta = n(2\pi/S_s)$, $k_\xi = \chi k_\eta$, and

$$\chi = \frac{M_{s,\xi}M_{s,\eta} \pm \sqrt{M_s^2 - 1}}{1 - M_{s,\xi}^2}$$

is a compressibility factor with the plus-or-minus sign chosen such that $\Phi_{\pm\infty} = 0$.

As a result of the relative motion, this spatially periodic potential field associated with the stator vanes induces velocities that are temporal excitations to the adjacent rotor-blade row. Thus, the induced velocity fields due to the upstream and downstream vane rows must be specified in a coordinate system attached to the rotor-blade row where the disturbances are unsteady. The vane rows are assumed to be identical and the repeating stage assumption is made. The reference position of the vane rows relative to one another is such that the leading edges of the airfoils in the upstream and downstream vane rows coincide at the same tangential position. With the rotor-blade row modeled as a flat-plate airfoil cascade, the initial positions of the three airfoil rows are as depicted in Fig. 3. At $t = 0$, the centerline of the wake shed by the upstream vane row intersects the leading edge of the reference airfoil of the downstream rotor blade. The transformation from the absolute ξ-η coordinate system fixed to the stator to the relative X-Y coordinate system attached to the responding rotor-blade row is

$$\xi = X\cos\Theta_r - Y\sin\Theta_r \tag{12a}$$

$$\eta = X\sin\Theta_r + Y\cos\Theta_r + U_w t \tag{12b}$$

The velocity potentials of the stator vane rows in a reference frame attached to the rotor is obtained by substituting Eqs. (12) into Eq. 11, with the velocity potentials for the nth harmonic given by

$$\Phi_{\mathrm{up}} = \bar{\Phi}_{\mathrm{up}}\exp\{i[k_\xi(\Delta\xi_{\mathrm{up}} + X\cos\Theta_r - Y\sin\Theta_r) + k_\eta(\Delta\eta_{\mathrm{up}} + X\sin\Theta_r + Y\cos\Theta_r + U_w t)]\} \tag{13a}$$

$$\Phi_{\mathrm{dn}} = \bar{\Phi}_{\mathrm{dn}}\exp\big(i\{k_\xi[-\Delta\xi_{\mathrm{dn}} + (X - C_r)\cos\Theta_r - Y\sin\Theta_r] + k_\eta[\Delta\eta_{\mathrm{dn}} + (X - C_r)\sin\Theta_r + Y\cos\Theta_r + U_w t]\}\big) \tag{13b}$$

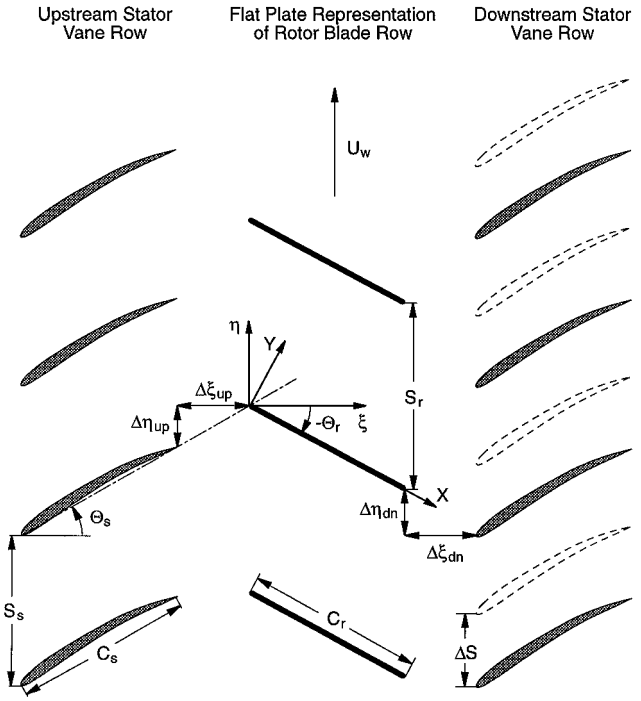

Fig. 3 Initial position of rotor and stator airfoil rows.

where $\bar{\Phi}_{up}$ and $\bar{\Phi}_{dn}$ are the complex amplitudes of the nth harmonic of the perturbation potentials due to the upstream and downstream vane rows evaluated at the vane trailing and leading edges, $\Delta\xi_{up}$ and $\Delta\xi_{dn}$ are the axial spacings between the rotor and the upstream and downstream stators, and $\Delta\eta_{up}$ and $\Delta\eta_{dn}$ are phase-shifting constants corresponding to the initial position depicted in Fig. 3 with

$$\Delta\eta_{up} = \Delta\xi_{up} \tan\Theta_s \tag{14a}$$

$$\Delta\eta_{dn} = \Delta\eta_{up} + C_r \sin\Theta_r + C_s \sin\Theta_s \tag{14b}$$

The induced velocities due to the potential fields of the upstream and downstream vane rows described by Eqs. (13) are obtained by taking the gradient of the potential functions with respect to the relative X-Y coordinate system, with the normal component given by

$$w = \frac{\partial\Phi}{\partial Y}$$

As the responding rotor-blade row is modeled as a flat-plate airfoil cascade (Fig. 2), these upwash velocities must vanish at the airfoil surfaces specified by

$$X = x + mS_r \sin\Theta_r, \qquad 0 \le x \le C_r \tag{15a}$$

$$Y = mS_r \cos\Theta_r \tag{15b}$$

where m is an index defining the location of each airfoil in the rotor cascade.

The resulting equation for the transverse component of the upwash on any rotor blade is

$$w_{up} = \bar{w}_{up} \exp\{i[k_\xi(\Delta\xi_{up} + x\cos\Theta_r) + k_\eta(\Delta\eta_{up} + x\sin\Theta_r) + m\sigma + \omega t]\} \tag{16a}$$

$$w_{dn} = \bar{w}_{dn} \exp(i\{k_\xi[-\Delta\xi_{dn} + (x - C_r)\cos\Theta_r] + k_\eta[\Delta\eta_{dn} + (x - C_r)\sin\Theta_r] + m\sigma + \omega t\}) \tag{16b}$$

where $\bar{w}_{up}$ and $\bar{w}_{dn}$ are the complex amplitudes of the upwash velocities normal to the rotor-blade chord line at the locations of the upstream stator vane trailing edge and downstream stator vane leading edge, respectively.

The upwash velocity on a rotor blade due to the viscous wake shed by the upstream stator vane row is modeled as a simply convected vortical gust:

$$w_w = \bar{w}_w \exp[i(-\omega/W_{r,\infty}x + m\sigma + \omega t)] \tag{17}$$

where $\bar{w}_w$ is the amplitude of the upwash velocity perturbation due to the wake at the location of the rotor-blade leading edge.

With the potential and vortical wake upwash velocity fields specified, the unsteady pressure difference coefficients for the rotor blades can be calculated from Eq. (9). The unsteady lift and moment coefficients then are computed by integration:

$$C_{L,w} = \frac{\text{Lift}}{\rho_\infty W_{r,\infty}^2 C_r(\bar{w}_w/W_{r,\infty})}, \qquad C_{M,w} = \frac{\text{Moment}}{\rho_\infty W_{r,\infty}^2 C_r^2(\bar{w}_w/W_{r,\infty})} \tag{18a}$$

$$C_{L,up} = \frac{\text{Lift}}{\rho_\infty W_{r,\infty}^2 C_r(\bar{w}_{up}/W_{r,\infty})}, \qquad C_{M,up} = \frac{\text{Moment}}{\rho_\infty W_{r,\infty}^2 C_r^2(\bar{w}_{up}/W_{r,\infty})} \tag{18b}$$

$$C_{L,dn} = \frac{\text{Lift}}{\rho_\infty W_{r,\infty}^2 C_r(\bar{w}_{dn}/W_{r,\infty})}, \qquad C_{M,dn} = \frac{\text{Moment}}{\rho_\infty W_{r,\infty}^2 C_r^2(\bar{w}_{dn}/W_{r,\infty})} \tag{18c}$$

Vane-Row Indexing Analysis

In the vane-row indexing technique, the numbers of stator vanes in the upstream and downstream vane rows are identical, with the downstream vane row indexed circumferentially relative to the upstream vane row (Fig. 3). The initial position of the vane rows relative to one another is such that the leading edges of the upstream and downstream stator vanes coincide at the same tangential position.

The unsteady aerodynamic forcing functions acting on the rotor-blade row are the potential flowfields of both the upstream and downstream vane rows, and the viscous wakes are generated by the airfoils in the upstream vane row. In a linearized analysis, the principle of superposition applies and the response of the rotor-blade row is the linear superposition of the responses to each individual forcing function. Thus, the total complex unsteady lift and moment coefficients are

$$C_L = \frac{\text{Lift}}{\rho_\infty W_{r,\infty}^2 C_r} = \frac{\bar{w}_w}{W_{r,\infty}} C_{L,w} + \frac{\bar{w}_{up}}{W_{r,\infty}} C_{L,up} + \frac{\bar{w}_{dn}}{W_{r,\infty}} C_{L,dn} \tag{19a}$$

$$C_M = \frac{\text{Moment}}{\rho_\infty W_{r,\infty}^2 C_r^2} = \frac{\bar{w}_w}{W_{r,\infty}} C_{M,w} + \frac{\bar{w}_{up}}{W_{r,\infty}} C_{M,up} + \frac{\bar{w}_{dn}}{W_{r,\infty}} C_{M,dn} \tag{19b}$$

where $\bar{w}_w$, $\bar{w}_{up}$, and $\bar{w}_{dn}$ represent the complex first harmonic amplitudes of the upwash velocities as determined from a Fourier analysis of each forcing-function waveform.

Both of the above expressions for the airfoil response can be expressed in terms of amplitudes and phase angles:

$$Ae^{i\theta} = A_w e^{i\theta_w} + A_{up} e^{i\theta_{up}} + A_{dn} e^{i\theta_{dn}} \tag{20}$$

where θ is the phase angle of the total unsteady lift or moment coefficient, and the amplitude A of the total response is

$$A^2 = (A_w\cos\theta_w + A_{up}\cos\theta_{up} + A_{dn}\cos\theta_{dn})^2 + (A_w\sin\theta_w + A_{up}\sin\theta_{up} + A_{dn}\sin\theta_{dn})^2 \tag{21}$$

The amplitudes and phase angles in the above equation correspond to the initial position depicted in Fig. 3. By indexing the vane rows relative to one another, only the phase angle of the rotor-blade response to the downstream vane-row potential field θ_{dn} is altered. Thus, by proper indexing of the vane rows, the total response of the rotor blades to all three forcing functions can be minimized. The maximum and minimum responses occur when the first derivative

of A^2 with respect to θ_{dn} is equal to zero, which yields the following critical values for θ_{dn}:

$$\tan\theta^*_{dn} = \frac{A_w \sin\theta_w + A_{up}\sin\theta_{up}}{A_w\cos\theta_w + A_{up}\cos\theta_{up}} \tag{22}$$

The minimum response occurs when the second derivative of A^2 with respect to θ_{dn} is positive, i.e., $A_w A_{dn}\cos(\theta_w - \theta^*_{dn}) + A_{up}A_{dn}\cos(\theta_{up} - \theta^*_{dn}) < 0$, and the maximum response when the second derivative is negative, i.e., $A_w A_{dn}\cos(\theta_w - \theta^*_{dn}) + A_{up}A_{dn}\cos(\theta_{up} - \theta^*_{dn}) > 0$.

The indexing position that yields the minimum total response is

$$\frac{\Delta S}{S_s} = \frac{\theta_{dn} - \theta^*_{dn}}{2\pi} \tag{23}$$

where ΔS is the distance from the initial position that the downstream vane row must be indexed as depicted in Fig. 3, θ_{dn} is the phase angle of the airfoil response due to the downstream vane-row potential field corresponding to the initial unindexed position, and θ^*_{dn} is the phase angle required to achieve the minimum response [Eq. (22)].

Results

To demonstrate vane-row indexing for passive flow-induced vibration control, the model developed herein is applied to a baseline stator–rotor–stator configuration. The upstream and downstream vane rows are identical, with the geometry of the three blade rows specified in Table 1. The results are presented in terms of an amplitude ratio, defined as the ratio of the amplitude of the airfoil response at the close spacing to that which would exist if the blade rows were spaced far apart, i.e., the wake response, vs vane indexing position.

The expressions for the complex unsteady lift and moment coefficients given by Eqs. (19) require values for the amplitudes of the three forcing functions. These amplitudes can be determined from a Fourier analysis of each forcing-function waveform and are complex quantities that contain phase as well as magnitude information. In general, these amplitudes depend upon both the airfoil geometry and the aerodynamic inlet conditions to the blade row generating the forcing function. For a particular airfoil geometry, the wake profile can be determined from Navier–Stokes solutions or a suitable wake correlation, and the potential-field-generated upwash from steady potential flow or computational fluid dynamics solutions.

For the present analysis, the magnitudes of the first harmonic velocity perturbations are assumed to be 10, 5, and 15% of the mean flow through the stator vane row for the wake, upstream potential, and downstream potential-field forcing functions, i.e., $|w_w|/W_{s,\infty} = 0.10$, $|w_{up}|/W_{s,\infty} = 0.05$, and $|w_{dn}|/W_{s,\infty} = 0.15$. These values were selected on the basis of experimental data from Ref. 8 and the numerical results presented in Ref. 9. These nondimensional velocity perturbations can be expressed in terms of the rotor relative velocity $W_{r,\infty}$ by noting that $W_{r,\infty}\cos\Theta_r = W_{s,\infty}\cos\Theta_s$. The approximate relationship developed in the Appendix shows that the phase angle for each of these forcing functions is 180 deg.

Figures 4 and 5 show the variation in unsteady lift over one indexing cycle as a function of axial spacing for rotor relative Mach numbers of 0.1 and 0.7, respectively. The results for $\Delta\eta/S_s = 0$ show the effect of simply decreasing the axial spacing between the blade rows without indexing the stator vanes. At the low Mach number, the response amplitude decreases as the axial spacing is decreased; at the high Mach number it decreases and then begins to increase again. This trend is counterintuitive because the axial spacing usually is increased to reduce resonant stress amplitudes to acceptable levels. However, these results may be unique with regard to this particular geometry and are a result of the strong potential-field interactions that occur between such closely spaced blade rows. For both Mach numbers, indexing has a maximum effect at the closest spacing, with near complete cancellation of the unsteady lift possible at the low Mach number. In contrast, at the high Mach number, the minimum response occurs at the 30% chord axial spacing, even though indexing has a larger impact at the closest spacing. The reason for this behavior is that for the high Mach number the response due to the downstream forcing function is dominant at the close spacing, whereas it is nearly equal to the amplitude of the combined response due to the upstream forcing functions at the low Mach number. Note that the minimum unsteady lift amplitude occurs near the unindexed position of the vane rows.

Table 1 Multistage blade-row configuration

Rotor stagger angle, Θ_r	−45 deg
Stator stagger angle, Θ_s	+45 deg
Rotor solidity, C_r/S_r	0.67
Stator solidity, C_s/S_s	1.0
Pitch ratio, S_r/S_s	1.5
Chord ratio, C_r/C_s	1.0
Rotor reduced frequency, k	8.89
Rotor interblade phase angle, σ	+540 deg

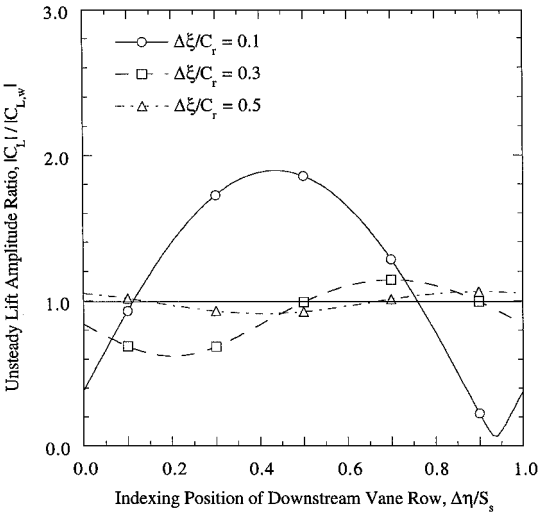

Fig. 4 Unsteady lift variation as a function of axial spacing ($M_r = 0.1$).

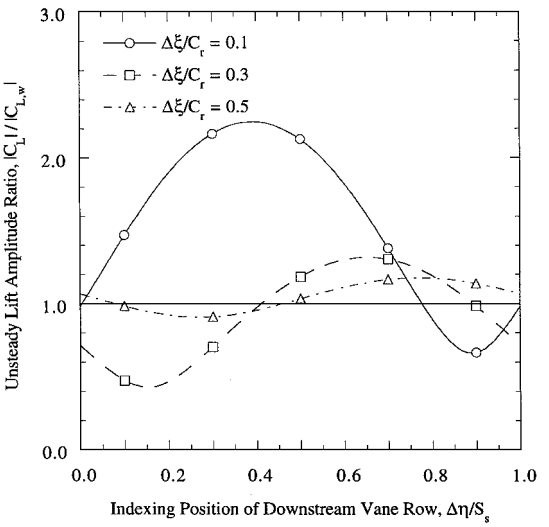

Fig. 5 Unsteady lift variation as a function of axial spacing ($M_r = 0.7$).

To achieve complete cancellation of the unsteady lift, the amplitude of the combined response to the upstream forcing functions must be equal to the amplitude of the response to the downstream forcing function. Figure 6 shows the amplitudes of the combined upstream vortical–potential response and the downstream potential response as functions of axial spacing for the low and high Mach numbers. Optimum combinations of upstream and downstream rotor–stator axial spacings that result in complete cancellation of the unsteady lift occur at points where the response

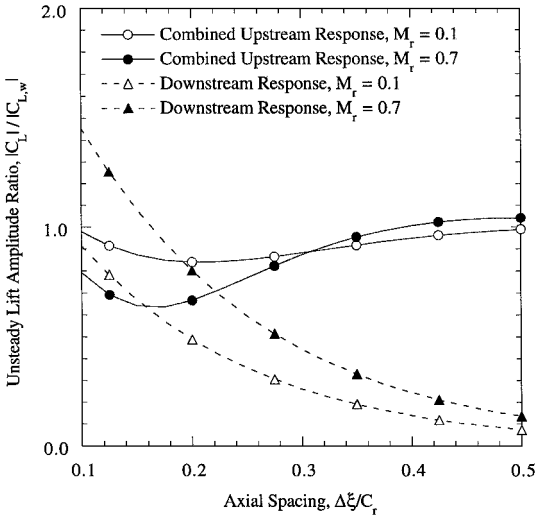

Fig. 6 Upstream and downstream response amplitudes as functions of axial spacing.

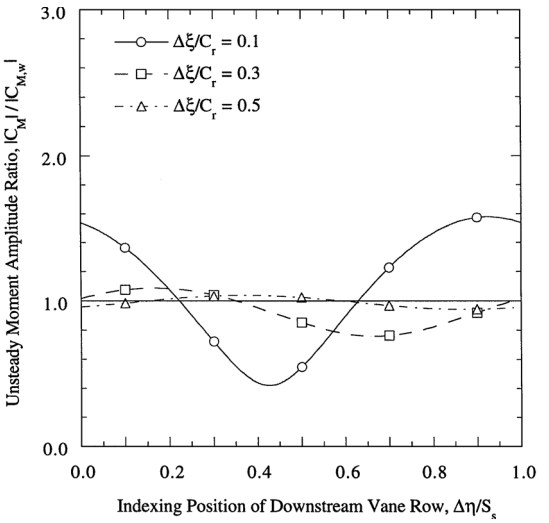

Fig. 8 Unsteady moment variation as a function of axial spacing ($x_{ea}/C_r = 0.5$, $M_r = 0.1$).

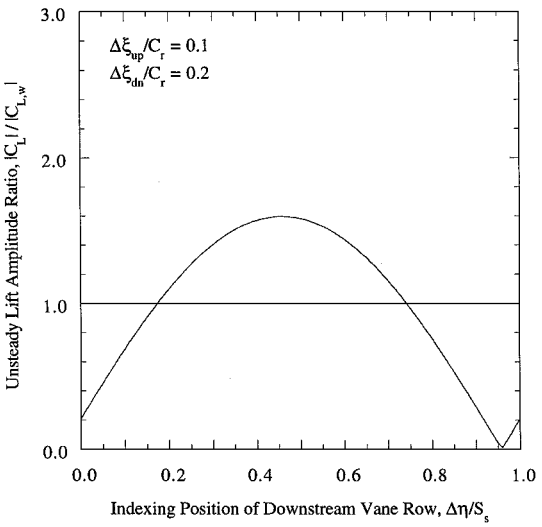

Fig. 7 Unsteady lift variation at an optimum axial spacing ($M_r = 0.7$).

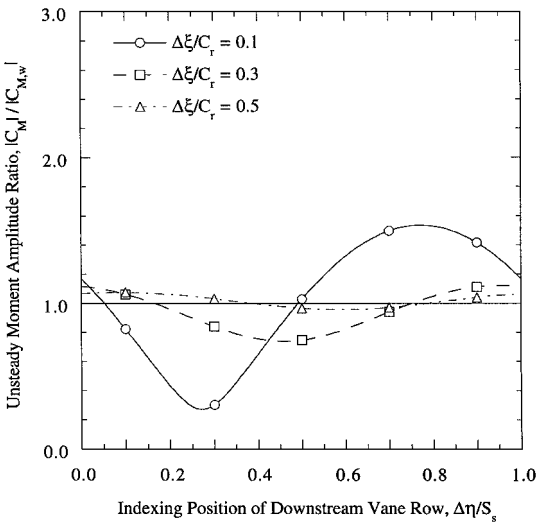

Fig. 9 Unsteady moment variation as a function of axial spacing ($x_{ea}/C_r = 0.5$, $M_r = 0.7$).

amplitudes are equal. At the low Mach number, near complete cancellation of the unsteady lift is only possible at the closest spacing, with the upstream combined vortical–potential response dominant at the larger spacings. In contrast, at the high Mach number, the downstream potential response is dominant for axial spacings less than 20% chord, whereas the combined upstream response is dominant for axial spacings greater than 20% chord. Thus, at the high Mach number, there are several possible combinations of upstream and downstream rotor–stator axial spacings that will yield nearly equal response amplitudes and thus allow near complete cancellation of the unsteady lift. One such combination would be an upstream rotor–stator axial spacing of 10% chord and a downstream rotor–stator axial spacing of 20% chord (Fig. 7). Note that the indexing position for complete cancellation of the unsteady lift is defined distinctly, with the response sharply approaching zero as this position is approached. This trend also was present in the low Mach number response at the closest axial spacing (Fig. 4).

Figures 8 and 9 show the variation in the unsteady moment amplitude over one indexing cycle as a function of the axial spacing for the low and high Mach numbers, respectively, with the rotor-blade elastic axis located at midchord. For both Mach numbers, the indexing position for the minimum moment response corresponds to that for maximum lift and vice versa (Figs. 4 and 5). Also note that the maximum moment response occurs near the unindexed position. For this configuration, indexing is most effective at the closest spacing, with reductions in amplitude of nearly 60 and 80% possible for the low and high Mach numbers, respectively. At the larger axial spacings, indexing does not significantly alter the response amplitude.

The centroid of the loading distribution for a symmetric cambered airfoil at zero angle of attack is at midchord, whereas for an uncambered airfoil at a finite angle of attack, it is located at the quarter-chord. For a fixed stator geometry, the upwash velocity due to camber loading will be the same both upstream and downstream of the blade row, whereas for angle of attack or incidence loading, the upwash will be much larger upstream of the blade row than downstream because of the exponential decay rate of the potential field [Eq. (11)]. Thus, varying the amplitude of the downstream forcing function qualitatively simulates the effects of increasing the incidence loading on the stator vane rows.

Figures 10 and 11 show the variation in the unsteady lift at the close axial spacing for the low and high Mach numbers, respectively, as the amplitude of the downstream velocity perturbation is varied from 5 to 15% of the mean stator velocity. At the low Mach number, the reduction in unsteady lift is strongly dependent on the stator-vane incidence loading, with near complete cancellation possible only for the largest downstream forcing-function amplitude. At the high Mach number, indexing the vane rows results in a significant reduction in the unsteady lift amplitude over that which corresponds to the wake response for all of the downstream vane

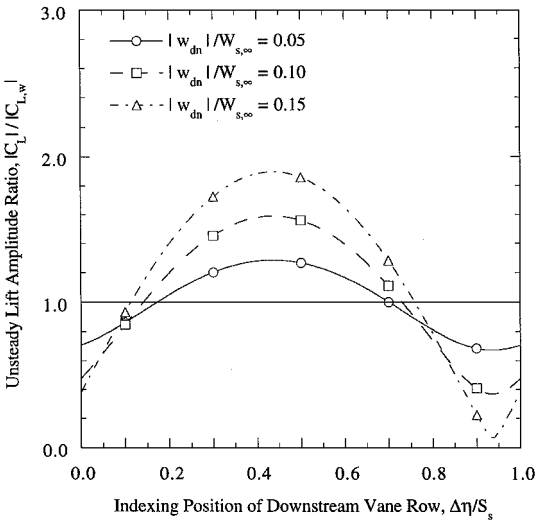

Fig. 10 Unsteady lift variation as a function of steady vane loading ($\Delta\xi/C_r = 0.1, M_r = 0.1$).

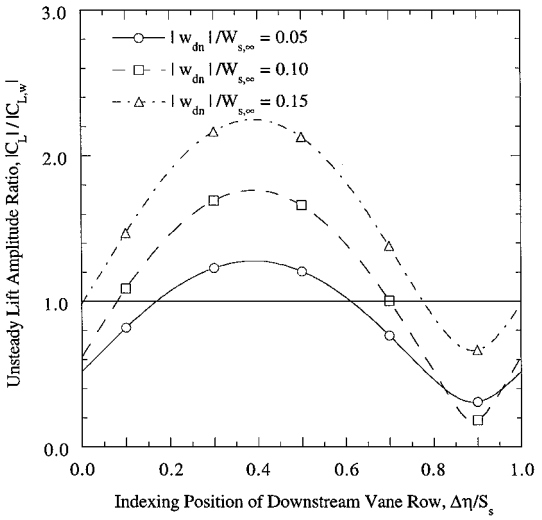

Fig. 11 Unsteady lift variation as a function of steady vane loading ($\Delta\xi/C_r = 0.1, M_r = 0.7$).

incidence loadings. Thus, for high Mach numbers, indexing has a large impact on the unsteady lift response even for modest values of vane incidence.

Figures 12 and 13 show the variation in the unsteady moment as a function of the downstream forcing-function amplitude at the close axial spacing for the low and high Mach numbers, respectively. The results are similar for both Mach numbers, with indexing being most effective for the largest forcing-function amplitude. The behavior for the high Mach number moment response thus differs from that noted for the lift response in which increasing the downstream forcing-function amplitude mainly caused the mean value of the unsteady lift over the indexing cycle to increase (Fig. 11).

Figure 14 shows the effect of varying the position of the elastic axis 10% forward and 10% aft of midchord for the high Mach number at the close spacing. To illustrate the effects of elastic-axis position on the response, the amplitude of the unsteady moment has been nondimensionalized by the amplitude of the wake response for an elastic axis located at the midchord position. Moving the elastic axis forward of midchord causes the maximum moment response to increase by nearly 10%. Similarly, moving the elastic axis aft of midchord results in a 10% decrease in the maximum response. Thus, if excessive torsional vibrations occur when the vane rows are indexed for minimum lift, moving the elastic axis aft of midchord may reduce the vibration amplitude to acceptable levels.

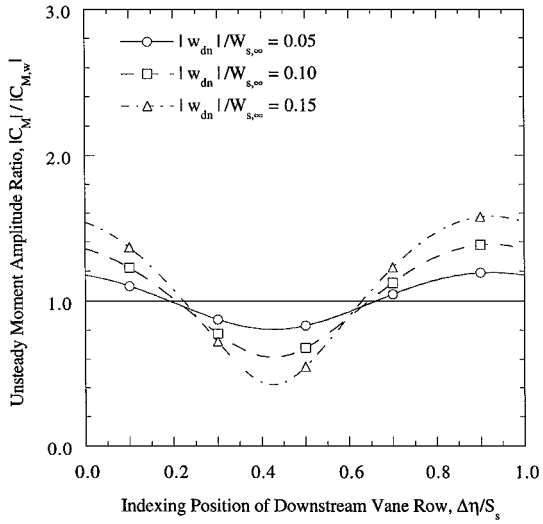

Fig. 12 Unsteady moment variation as a function of steady vane loading ($x_{ea}/C_r = 0.5, \Delta\xi/C_r = 0.1, M_r = 0.1$).

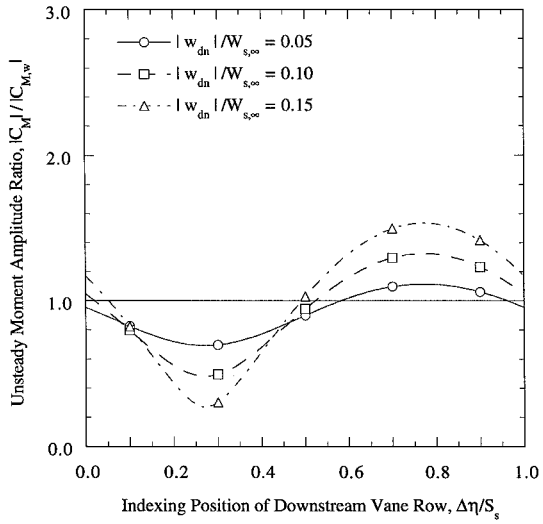

Fig. 13 Unsteady moment variation as a function of steady vane loading ($x_{ea}/C_r = 0.5, \Delta\xi/C_r = 0.1, M_r = 0.7$).

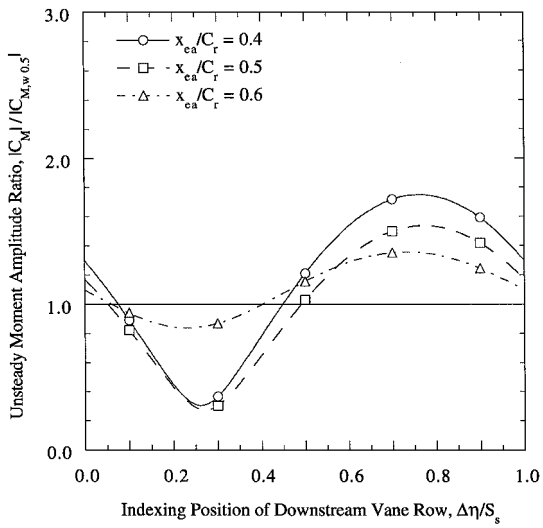

Fig. 14 Unsteady moment variation as a function of elastic-axis location ($\Delta\xi/C_r = 0.1, M_r = 0.7$).

Summary and Conclusions

A mathematical model to predict the effectiveness of vane-row indexing as a passive vibration control technique has been developed. This was accomplished by extending a compressible flat-plate cascade analysis to account for the induced velocities due to potential-field interactions. The unsteady aerodynamic coefficients obtained from this model then were used in a vane-row indexing analysis to determine the resulting unsteady aerodynamic response of a baseline stator–rotor–stator configuration.

For the particular geometry analyzed, both the minimum unsteady lift and the maximum unsteady moment responses occurred near the unindexed position of the stator vane rows; simply decreasing the axial spacing markedly affected the unsteady aerodynamic response. However, by indexing the stator vanes, significant reductions in the unsteady lift and moment could be achieved at the close spacings. At the closest spacing, near complete cancellation of the unsteady lift was possible at the low Mach number. At the high Mach number, there were optimum combinations of upstream and downstream rotor–stator axial spacings that could result in complete cancellation of the unsteady lift. However, even for a moderate axial spacing of 30% chord, up to a 60% reduction in the unsteady lift over that of the wake response was obtained.

With the rotor-blade elastic axis located at midchord, the indexing position for minimum lift corresponded to that for maximum moment, and vice versa. Thus, for this particular geometry, vane-row indexing cannot be used to minimize both the unsteady lift and moment. However, moving the elastic axis forward of midchord resulted in an increase in the moment response, whereas moving it aft of midchord resulted in a decrease in the response. Thus, at the indexing position corresponding to minimum lift, there may be an optimum location of the elastic axis that would also result in a low moment response.

Vane-row indexing has been shown to be a viable technique for the passive control of rotor-blade flow-induced vibrations, with it being most effective for close axial spacings. Thus, this technique may not only increase component durability by decreasing the unsteady aerodynamic blade loading, but also may allow the use of more closely spaced blade rows than currently used in gas turbine engines.

Appendix: Upwash Velocity Phase

The viscous wake is a velocity deficit with a maximum amplitude occurring along the wake centerline, with the axial and tangential velocity perturbations given by

$$\bar{u} = -|w_w| \cos \Theta_s \tag{A1a}$$

$$\bar{v} = -|w_w| \sin \Theta_s \tag{A1b}$$

where $|w_w|$ denotes the wake velocity deficit magnitude in the absolute reference frame.

The component of the upwash velocity normal to the rotor-blade chord line is

$$\bar{w} = \bar{v} \cos \Theta_r - \bar{u} \sin \Theta_r \tag{A2}$$

Substituting Eq. (A1) into Eq. (A2) gives the upwash velocity due to an upstream viscous wake. For the configuration analyzed in this paper, $\sin \Theta_r = -\cos \Theta_s$ and $\cos \Theta_r = \sin \Theta_s$, and thus $\bar{w}_w = -|w_w|$.

Experimental data and numerical results indicate that along the leading- and trailing-edge locuses of a blade row, the static pressure perturbation due to the potential field is nearly sinusoidal, with a maxima at or very near the leading and trailing edges, and a minima near midpitch (see, e.g., Fig. 8 of Ref. 8). The exact location and amplitude of this static pressure perturbation generally depends on both the airfoil geometry and the aerodynamic inlet conditions to the blade row and will be different in the upstream and downstream directions. As an approximation, the maximum perturbation pressure is assumed to be located at the airfoil leading and trailing edges. The velocity perturbations are related to the static pressure perturbation by substituting Eq. (3) into the momentum equation (2). Because the flow through the stator vane row is steady, the time dependence is neglected, resulting in the following axial and tangential velocity perturbations due to the potential field of a blade row:

$$\bar{u} = \frac{-\chi \bar{p}}{\rho_\infty W_{s,\infty} (\chi \cos \Theta_s + \sin \Theta_s)} \tag{A3a}$$

$$\bar{v} = \frac{-\bar{p}}{\rho_\infty W_{s,\infty} (\chi \cos \Theta_s + \sin \Theta_s)} \tag{A3b}$$

Substituting Eq. (A3) into Eq. (A2) relates the complex static pressure perturbation and upwash velocity amplitudes. At the airfoil leading and trailing edges, the static pressure perturbation is a maximum; thus the complex upwash velocity amplitude is

$$\frac{\bar{w}}{W_{s,\infty}} = \frac{|\bar{p}|}{\rho_\infty W_{s,\infty}^2} \frac{(-\cos \Theta_r + \chi \sin \Theta_r)}{(\chi \cos \Theta_s + \sin \Theta_s)} \tag{A4}$$

For the configuration analyzed in this paper, $\sin \Theta_r = -\cos \Theta_s$ and $\cos \Theta_r = \sin \Theta_s$, so that Eq. (A4) simplifies to

$$\frac{\bar{w}}{W_{s,\infty}} = \frac{-|\bar{p}|}{\rho_\infty W_{s,\infty}^2} \tag{A5}$$

Thus, the normal component of the upwash velocity is 180 deg out of phase with the static pressure perturbation. Because the maximum static pressure perturbation is assumed to occur at the airfoil leading and trailing edges, $\bar{w}_{\text{up}} = -|w_{\text{up}}|$ and $\bar{w}_{\text{dn}} = -|w_{\text{dn}}|$, where $|w_{\text{up}}|$ and $|w_{\text{dn}}|$ represent the magnitudes of the upwash velocity due to the upstream and downstream vane-row potential fields, respectively.

Acknowledgments

This research was sponsored, in part, by the Army Research Office (ARO). This support is most gratefully acknowledged.

References

[1]Dring, R. P., Joslyn, H. D., Hardin, L. W., and Wagner, J. H., "Turbine Rotor-Stator Interaction," *Journal of Engineering for Gas Turbines and Power*, Vol. 104, No. 4, 1982, pp. 729–742.

[2]Smith, L. H., "Casing Boundary Layers in Multistage Axial-Flow Compressors," *Flow Research in Blading*, edited by L. S. Dzung, Elsevier, Amsterdam, 1970, pp. 275–299.

[3]Walker, G. J., and Oliver, A. R., "The Effect of Interaction Between Wakes from Blade Rows in an Axial Flow Compressor on the Noise Generated by Blade Interaction," *Journal of Engineering for Power*, Vol. 94, No. 3, 1972, pp. 241–248.

[4]Schmidt, D. P., and Okiishi, T. H., "Multistage Axial-Flow Turbomachine Wake Production, Transport, and Interaction," *AIAA Journal*, Vol. 15, No. 8, 1977, pp. 1138–1145.

[5]Capece, V. R., and Fleeter, S., "Unsteady Aerodynamic Interactions in a Multistage Compressor," *Journal of Turbomachinery*, Vol. 109, No. 3, 1987, pp. 420–428.

[6]Dorney, D. J., and Sharma, O. P., "A Study of Turbine Performance Increases Through Airfoil Clocking," AIAA Paper 96-2816, July 1996.

[7]Smith, S. N., "Discrete Frequency Sound Generation in Axial Flow Turbomachines," British Aeronautical Research Council, R&M 3709, London, 1972.

[8]Johnston, R. T., Feiereisen, J. M., and Fleeter, S., "High Speed Axial Fan Stage Wakes for Application to Flow Induced Vibration Prediction," AIAA Paper 94-2975, June 1994.

[9]Korakianitis, T., "On the Propagation of Viscous Wakes and Potential Flow in Axial-Turbine Cascades," *Journal of Turbomachinery*, Vol. 115, No. 1, 1993, pp. 118–127.